Solution Structure of LSIII, a Long Neurotoxin from the Venom of *Laticauda semifasciata*[†,‡]

Peter J. Connolly,* Alan S. Stern, and Jeffrey C. Hoch*

The Rowland Institute for Science, 100 Edwin H. Land Boulevard, Cambridge Massachusetts 02142

Received August 25, 1995; Revised Manuscript Received November 14, 1995[⊗]

ABSTRACT: We report the sequence-specific proton assignments and solution structure of the long neurotoxin LSIII from the venom of *Laticauda semifasciata* determined by two- and three-dimensional ^{1}H NMR. Input for structure calculations consisted of 497 NOE-derived distance restraints and 45 dihedral angle restraints obtained from J couplings. A two-particle-per-residue representation of protein structure was used to generate 200 initial structures which were then subjected to all-atom refinement by simulated annealing. Twenty-three final structures consistent with the experimental restraints were obtained; the average atomic RMS difference between the individual structures and the mean structure was 0.82 Å for the backbone heavy atoms and 1.3 Å for all heavy atoms (residues 1−26, 37−60). The main elements of regular secondary structure are a three-stranded antiparallel β-sheet and three finger-like loops protruding from a globular core, consistent with previously reported structures of long neurotoxins. The end of the prominent loop II, which is involved in binding to acetylcholine receptor, is disordered relative to the rest of the molecule. A novel finding of this study is that the loop has a well defined local structure; this and other observations suggest this region moves as a rigid body. We propose that this motion is a heretofore unrecognized general feature of long neurotoxins, with specific consequences for binding to the acetylcholine receptor.

Neurotoxins are among the most lethal components found in the venom of fixed-front fanged snakes. These toxins bind with high affinity and selectivity to the nicotinic acetylcholine receptor (AChR)[1] in the postsynaptic membranes of nerve and skeletal muscle, blocking neuromuscular response and inducing flaccid paralysis. These postsynaptic neurotoxins can be classified into two general groups: short neurotoxins having four disulfide bridges and chain lengths of 60−62 residues, and long neurotoxins having a fifth disulfide bridge and chain lengths of 66−74 residues. Both classes of neurotoxins exhibit sequence homology and similar overall topologies, characterized by a three-stranded antiparallel β-sheet and three finger-like loops protruding from a globular core. These neurotoxins form one of the largest families of proteins whose primary structures are known, with approximately 80 amino acid sequences determined (Endo & Tamiya, 1987).

Neurotoxins have been the subject of intensive investigation not only due to interest in the development of therapeutic treatment for venomous snake bites but also because their affinity and specificity has proven invaluable for studies of AChR, whose atomic structure is not yet known. X-ray and NMR structural studies have been carried out on two long neurotoxins, α-cobratoxin (Walkinshaw et al., 1980; Betzel et al., 1991; La Goas et al., 1992) and α-bungarotoxin (Love & Stroud, 1986; Basus et al., 1988). The crystal and NMR structures of α-cobratoxin are in good agreement with one another but differ from the crystal structure of α-bungarotoxin. NMR studies of α-bungarotoxin suggest that the conformation is similar to that of α-cobratoxin.

In this paper we report the solution structure of the long neurotoxin, LSIII, from the venom of *Laticauda semifasciata*. The overall fold is similar to that of the other long neurotoxin structures. Consistent with previous studies, the end of the prominent central loop appears disordered relative to the rest of the molecule. Careful examination of the structure of this loop shows that it exhibits local order, which was not noted before. The local structure and dynamics of this highly conserved binding loop hold implications for receptor binding.

MATERIALS AND METHODS

NMR. LSIII was purchased from Sigma Chemical Co. and used without further purification. The number of cross peaks in the fingerprint region of the P.COSY spectrum, spectral line widths, and reverse-phase HPLC results were all consistent with a sample containing a single, monomeric protein. Samples were prepared in either 90% H_2O/10% D_2O or 99.9% D_2O at a concentration of 4.0 mM. The pH was adjusted to 4.6 (uncorrected for isotope effects) by the addition of NaOD and DCl.

All ^{1}H spectra were acquired using a JEOL GX400 spectrometer at 25 °C unless otherwise noted. P.COSY (Marion & Bax, 1988), DQF-COSY (Piantini et al., 1982; Shaka et al., 1983; Rance et al., 1983), and RELAY (Eich et al., 1982; Wagner, 1983; Bax & Drobny, 1985) spectra were acquired in both 90%H_2O/10%D_2O and 99.9% D_2O. Z-filtered TOCSY spectra (Rance, 1987) were recorded with 40, 50, and 70 ms mixing times using the DIPSI-2 (Rucker

[†] Supported by the Rowland Institute for Science. Computations were performed using facilities provided by a grant from the National Institutes of Health (GM-47467, Gerhard Wagner, P.I.).

[‡] Coordinates submitted to the Brookhaven Protein Data Bank (accession code 1LSI).

[⊗] Abstract published in *Advance ACS Abstracts,* December 15, 1995.

[1] Abbreviations: AChR, acetylcholine receptor; COSY, correlation spectroscopy; NOE, nuclear Overhauser effect; NOESY, nuclear Overhauser effect spectroscopy; RMSD, root-mean-square deviation; TOCSY, total correlation spectroscopy.

0006-2960/96/0435-418$12.00/0

& Shaka, 1989) isotropic mixing sequence. NOESY (Kumar et al., 1979) spectra were acquired using mixing times of 100 and 200 ms. A 3-D NOE-TOCSY spectrum (Vuister et al., 1988) was acquired using a 200 ms NOE mixing time and a 50 ms isotropic mixing period. The data for this experiment were collected as described by Cavanagh and Rance (1990) using a z-filtered DIPSI-2 isotropic mixing sequence. In all cases water suppression was achieved with presaturation during the recycle delay, except for NOESY spectra, where jump−return (Plateau & Gueron, 1982) was used. A 70 ms z-filtered TOCSY spectrum and an E.COSY spectrum (Griesinger et al., 1985) were acquired on a Bruker AMX 500 spectrometer. 2-D data were collected with either 1024 or 2048 complex points in t_2 and 256 or 512 complex points in t_1. For the 3-D NOE-TOCSY experiment, 64 complex points were acquired in t_1 and t_2, and 256 complex points were acquired in t_3. The spectral width was 5500 Hz for all experiments acquired at 400 MHz and 6225 Hz for the two spectra acquired at 500 MHz. All 400 MHz spectra were acquired in the pure-phase mode using the States−Haberkorn−Ruben method (States et al., 1982); data acquired at 500 MHz were collected using TPPI (Marion & Wüthrich, 1983).

Data were processed using the Rowland NMR Toolkit (Hoch & Stern, 1993). For P.COSY, DQF-COSY, and E.COSY spectra, trapezoidal apodization was used in t_1, and trapezoidal followed by Lorentzian-to-Gaussian apodization was used in t_2. For all other spectra, Lorentzian-to-Gaussian apodization was applied in the directly detected dimension and a 60°-shifted sine bell was used in the indirectly detected dimensions. In addition, filtering of low-frequency components in the time domain was used to reduce the residual water resonance (Marion & Bax, 1989). All spectra were zero-filled once in the directly detected dimension and twice in the indirectly detected dimension prior to Fourier transformation.

Experimental Restraints. Upper bounds for distance restraints were determined from the integrated cross peak volumes in a single NOE spectrum recorded with a 100 ms mixing time, using the program CALIBA (Güntert et al., 1991). A correction factor of 0.5 Å was added to the upper bound of distances involving methyl groups, and standard pseudoatom corrections were applied for methyl and methylene protons when stereospecific assignments were not available (Wüthrich et al., 1983). Hydrogen bond restraints in β-sheets consistent with preliminary structure calculations were identified by the characteristic pattern of interstrand NOEs and slowly exchanging amide protons. For each hydrogen bond identified, the N−O and H^N−O distances were constrained to the ranges of 2.4−3.3 Å and 1.7−2.3 Å, respectively. Disulfide bonds were assumed to be the same as for the homologous protein α-cobratoxin (3−20, 13−41, 26−30, 45−56, and 57−62), and the S^γ−S^γ distances were constrained to the range of 1.9−2.2 Å. (Several of these were confirmed by the observation of H^β−H^β NOEs.) $^3J_{\alpha N}$ coupling constants were determined by a nonlinear least-squares fit of the coupling constant, line width, and chemical shift to t_2 cross-sections in the P.COSY and DQF-COSY spectra using the program XPEAKFIT (Stern, 1994). For couplings larger than 8 Hz, the ϕ angle was restricted to the range (−170°, −70°), and for couplings smaller than 6 Hz the ϕ angle was restricted to the range (−90°, −40°). $^3J_{\alpha\beta}$ couplings were determined directly from the peak-to-peak separation in the E.COSY spectrum. Stereospecific assignment of the β protons and determination of χ_1 angle restraints were based on the analysis of these couplings, along with the H^N−H^β and H^α−H^β NOEs and examination of preliminary structures.

Structure Calculations. Three-dimensional structures were calculated on the basis of experimentally derived distance and angle restraints using X-PLOR (Brünger, 1992). Initially, 200 starting structures were generated by applying a simulated annealing protocol to a two-particle-per-residue representation (one to represent the α-carbon and another to represent the β-carbon or second α-hydrogen) of protein structure (Stern & Hoch, 1992). All-atom structures were derived from the two-particle structures by a least-squares fit for each residue using all-atom coordinates in a canonical configuration. The structures were then regularized by minimization. One hundred steps of Powell minimization were carried out using the bond and van der Waals energy terms together with the NOE and dihedral restraints. A further 100 steps of minimization were performed with the angle energy term included. These structures were then refined using a dynamical simulated annealing protocol similar to that described by Nilges et al. (1988). Nine picoseconds of dynamics were performed at 2000 K during which the improper torsion angle force constant was gradually increased from 0.1 to 1.0 kcal/M·deg^2 and the van der Waals force constant reduced from 20.0 to 0.003 kcal/M·Å^2. The system was then cooled linearly to 100 K over a period of 18 ps. The dihedral angle force constant was held at 5 kcal/M·deg^2 for the first 9 ps of cooling and then increased to 200 kcal/M·deg^2 while the van der Waals force constant was increased from 0.003 to 4.0 kcal/M·Å^2. Similarly, the van der Waals radius scale factor was decreased from 0.9 to 0.75. After cooling, 200 steps of Powell minimization were performed. A second stage of refinement used a similar protocol consisting of 6 ps of high temperature dynamics and 24 ps of cooling with the dihedral angle force constant held constant at 200 kcal/M·deg^2 throughout the cooling procedure. A final minimization was performed which included harmonic *J* restraints using a force constant of 1.0 kcal/M·Hz^2 for experimentally determined H^α−H^N couplings.

Initial structures were calculated using 398 distance restraints derived from resonances that could be unambiguously assigned in the 100 ms NOE spectra, using the low precision two-particle structure (Connolly et al., 1994) to resolve some of the ambiguous cross peaks. Restraints for the five disulfides were also included. On the basis of the resulting low energy structures, some ambiguities in the NOE spectrum could be resolved and additional distance restraints determined. Hydrogen bond restraints consistent with these initial structures and amide proton exchange data were included, along with ϕ angle restraints based on H^α−H^N coupling constants. A second set of structures was calculated and the procedure repeated until no further ambiguities in the NOE spectrum could be resolved based on the calculated structures. At each stage, the structures were examined for distance restraints that were consistently violated, and corrections for misassignments or spectral overlap were made as warranted. For the final structure refinements, 497 distance restraints were used, including 115 medium- and long-range restraints and 20 hydrogen-bond restraints, together with 31 ϕ and 14 χ_1 angle restraints. The final minimization also included 31 *J* restraints.

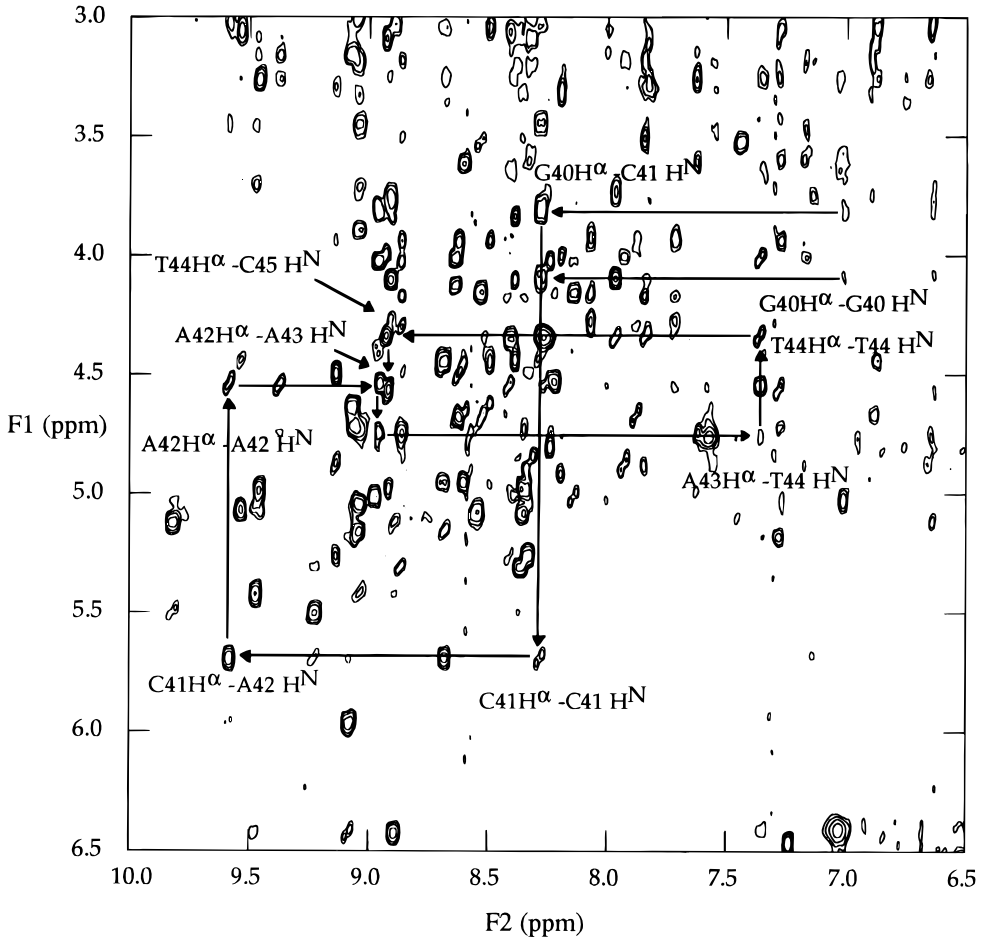

FIGURE 1: 400 MHz NOE spectrum (200 ms mixing time) of LSIII, pH 4.6, 25 °C in 90%H_2O/10%D_2O. Sequential $H^{\alpha}(i)-H^{N}(i+1)$ connectivities for G40−T45 are indicated with arrows.

RESULTS

Sequential Assignments. Sequential assignments were determined using the procedure of Wüthrich et al. (1986) aided by the interactive analysis program EASY (Eccles et al., 1991). The four glycine spin systems were easily identified by the unique fine structure of the $H^{\alpha}-H^{N}$ crosspeaks in the P.COSY spectrum. Four alanines were located from the $H^{\beta}-H^{N}$ methyl resonances in the RELAY spectrum. Four out of six serines were located by the unusual downfield shift of the β protons and five out of six threonines were identified by the correlation of a single downfield-shifted β proton to a methyl group. On the basis of downfield-shifted γ protons relative to the β protons, it was possible to classify four spin systems as either glutamine or glutamic acid residues, and the two valine residues were identified on the basis of a single β proton correlated to two γ methyl groups in the P.COSY spectrum. Three out of the four proline spin systems were located by their unique cross peak patterns in a TOCSY spectrum in D_2O. The remaining spin systems were classified as having short side chains (H^{β} only), having long side chains (H^{γ} or longer), containing a methyl group, or unknown.

Sequential assignments were made by identifying $H^{\alpha}(i)-H^{N}(i+1)$ or $H^{N}(i)-H^{N}(i+1)$ cross peaks in the 200 ms NOESY spectra collected in H_2O and D_2O. An example of the sequential $H^{\alpha}-H^{N}$ connectivities for residues 40−45 is shown in Figure 1, and the fingerprint region of a 400 MHz TOCSY spectrum is shown in Figure 2. Extensive use of the 3-D NOE-TOCSY spectrum was made to confirm assignments and to resolve overlap in the 2-D NOESY spectra. This was especially useful for correlating overlapping H^{α} resonances to well resolved amide protons. Observation of long-range interstrand NOEs, along with strong $H^{\alpha}(i)-H^{N}(i+1)$ and weak $H^{\alpha}(i)-H^{N}(i)$ NOEs, allowed the identification of a three-stranded antiparallel β sheet comprising residues 19−25, 37−42, and 52−58. These NOEs are shown in Figure 3. Out of all backbone NOEs expected of this triple stranded sheet, 78% were observed, 11% could not be unambiguously identified because of overlap, and the remainder were not observed. A summary of the sequential NOEs is shown in Figure 4. The resonance assignments are given in Table S1 (Supporting Information).

Structure Determination. The 23 lowest energy structures are shown in Figures 5 and 6. All of the structures are in good agreement with the experimental restraints, with no structure having NOE distance restraint violations greater than 0.5 Å or dihedral angle restraint violations greater than 5.0°. The structures have empirical energies less than 350 kcal/M and exhibit good covalent geometries, with RMS deviations from the canonical values of 0.004 Å for bond lengths and 0.75° for angles. Examination of Ramachandran plots for individual structures (not shown) showed that the backbone dihedral angles of nearly all residues lie in the allowed regions. Residues with unfavorable $\phi-\psi$ angles were in regions of poorly defined structure.

A comparison of structures minimized with and without *J* restraints showed only small differences in the atomic coordinates, and the precision of the structures, as measured

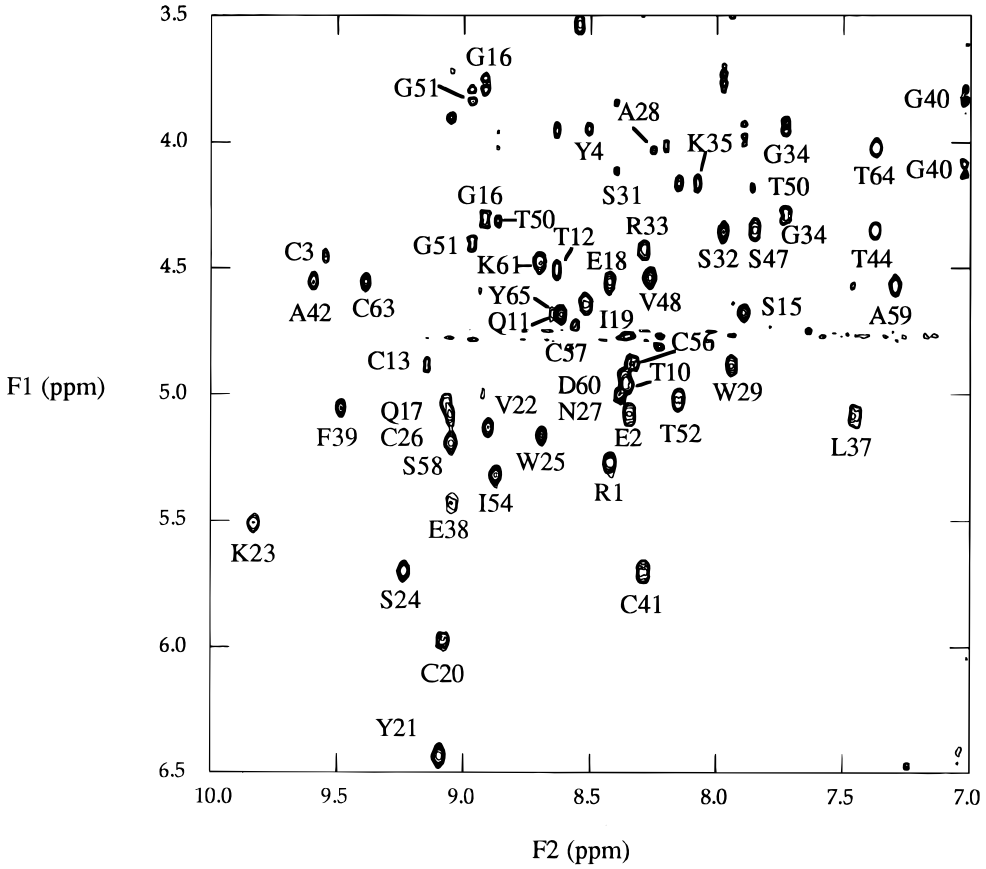

FIGURE 2: Fingerprint region of a 400 MHz TOCSY spectrum (40 ms mixing time) of LSIII, pH 4.6, 25 °C in 90%H_2O/10%D_2O. For clarity, only the $H^{\alpha}(i)-H^{N}(i)$ resonances are labeled.

by RMSD, was unaffected. The inclusion of the *J* restraint term significantly improved the agreement between experimentally determined $H^{\alpha}-H^{N}$ couplings and those computed from the refined structures. The RMSD between experimental and calculated couplings was 2.5 and 1.0 Hz for structures without and with *J* refinement. The average expected error in the determination of these couplings was 0.55 Hz. A comparison of observed and computed $H^{\alpha}-H^{N}$ couplings is given in Figure 7. Minimization of individual structures using the CHARMM 22 force field (Molecular Simulations, Inc., 1994) gave negative Lennard-Jones energies (-408 ± 10 kcal/M) with negligible shifts in atomic positions (backbone RMSD < 0.2 Å), indicating good nonbonded contacts. Statistics for the family of structures are given in Table 1, and the RMSDs per residue are shown in Figure 8.

DISCUSSION

Description of the Structure. The main element of regular secondary structure is a three-stranded antiparallel β-sheet consisting of residues 19−25, 37−42, and 52−58. The structure is well defined in this region by a large number of interstrand NOEs as well as a characteristic pattern of strong sequential and weak intraresidue $H^{\alpha}-H^{N}$ NOEs. The RMSD for backbone heavy atoms in the β-sheet region is 0.26 Å. The side chain conformations of residues comprising the hydrophobic core of the β-sheet region are well defined by the NOE data and χ_1 angle restraints, as can be seen in Figure 6. The elements of regular secondary structure are connected mainly by loops, and the structure does not contain any readily classified turns.

A number of regions show high RMSDs relative to the well defined β-sheet. Residues 13−17 form the solvent-exposed loop near the beginning of the first strand of sheet; no long-range NOEs were observed for these amino acids. Residues 46−50, comprising part of the solvent-exposed region of loop III, also show a higher than average RMSD. Although there are a number of ϕ angle restraints for these residues, no long-range NOEs are observed. In addition, examination of the crystal structure of α-cobratoxin shows that there are no long-range proton pairs less than 5.0 Å apart in residues 42−48. These two observations suggest that the absence of NOEs in this region may be due more to molecular topology than to structural disorder. The end of loop II, which includes a number of highly conserved residues believed to be important in receptor binding (Endo & Tamiya, 1987), exhibits the highest RMSD values, with the exception of the carboxy terminus.

Local Structure at the End of Loop II. Closer examination of the residues comprising the end of loop II reveals that it exhibits local order and is only disordered with respect to the body of the protein. Superposition of residues 26−35 alone improves the backbone RMSD from 1.74 to 0.44 Å (Figure 8); by way of comparison, matching the disordered residues 1−10 reduces the RMSD from 1.18 (when residues 1−25 and 37−62 are matched) to 0.85 Å, a much smaller change. Examination of the backbone angular order parameters [as defined by Hyberts et al. (1992)] is more revealing and shows that the ϕ and ψ angles are well-defined for loop II, with the exception of ψ for Lys 27 and ϕ for Ala 28 (Figure 10). Each of these angles has two distinct values and the angles are correlated, suggesting that these residues

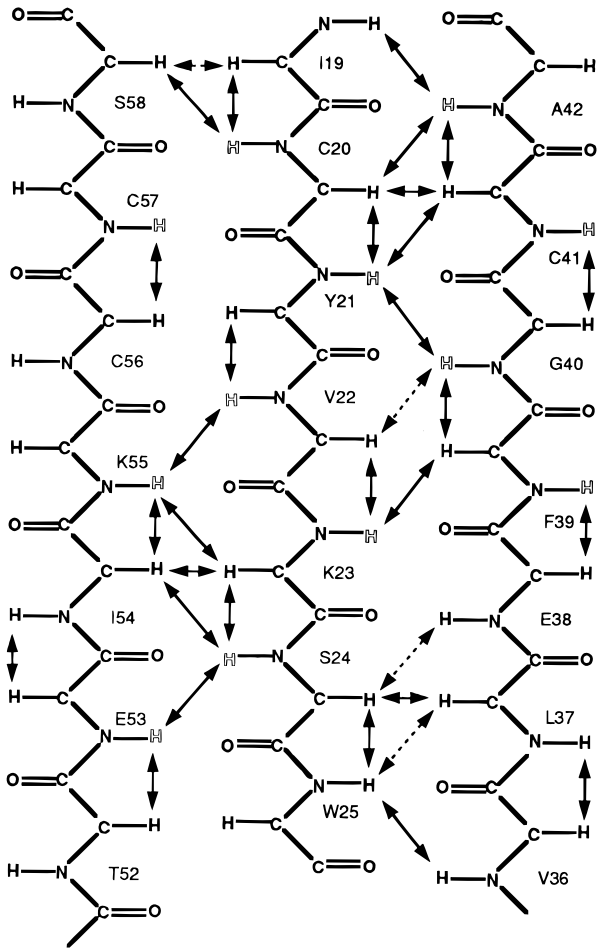

FIGURE 3: Schematic representation of the observed NOEs defining the three-stranded antiparallel β-sheet of LSIII. NOEs that could not be quantified are shown as a dotted-line arrow. Amide protons observed to be in slow exchange with solvent are indicated by H.

form a hinge having two preferred conformations. The empirical energies of the two conformers are nearly identical.

Motional averaging of vicinal coupling constants, whether through large fluctuations about a central value or through exchange between different values, tends to cause measured values to move away from the extremes of the Karplus relation (Hoch et al., 1985). Measured values that are close to the extremes can only occur when there is little conformational averaging or when exchange occurs between conformations with equivalent extreme values of the vicinal coupling. The $H^{\alpha}-H^{N}$ vicinal coupling constants for most of loop II fall outside the range (6−8 Hz) that is indicative of conformational averaging (Figure 7). In contrast, the value of 6.8 Hz for Ala 28 is in the range consistent with motional averaging (particularly since ϕ angles that give rise to vicinal coupling constants close to this value are energetically unfavorable). The average calculated $H^{\alpha}-H^{N}$ vicinal coupling constant for Ala 28 is 6.7 Hz, in excellent agreement with the experimentally observed coupling, and neither of the two preferred conformers alone would be expected to give rise to this coupling.

These observations are consistent with rigid-body motion of the end of loop II with respect to the rest of the protein, with the hinge localized to residues 27 and 28 on one side of the loop, but delocalized over several residues on the other side. The nuclear Overhauser effects observed within the loop provide strong evidence for local order, but they do

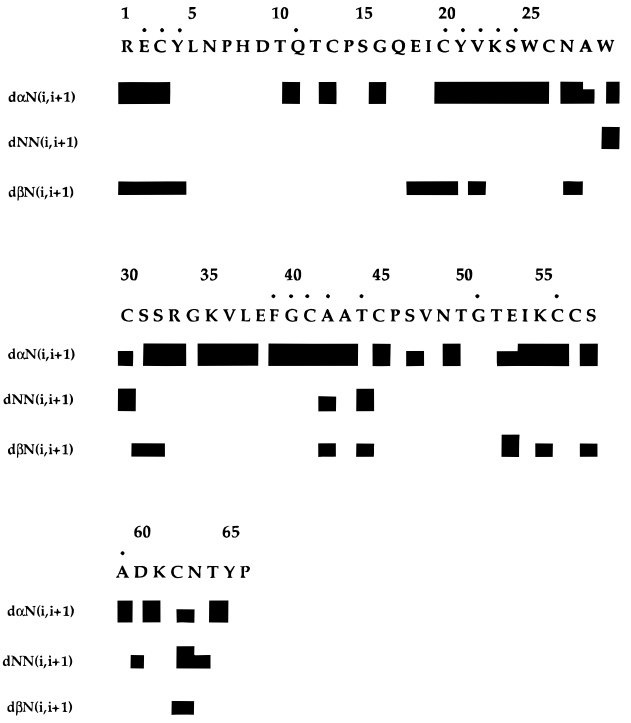

FIGURE 4: Summary of sequential NOEs involving H^{N}, H^{α}, and H^{β} for LSIII from a 200 ms NOE spectrum acquired at pH 4.6, 25 °C. Amide protons in slow exchange are indicated by "•".

not provide evidence for or against motion of the loop. It is well known that the absence of nuclear Overhauser effects is not sufficient to indicate motion, since there may be other reasons that NOEs are not observed (Hyberts et al., 1992). However, the vicinal coupling constants and chemical shifts are also consistent with rigid-body motion of loop II.

As a control, to explore the possibility that the structure in loop II is due to bias in the force field rather than the experimental restraints, we performed calculations in which the 79 restraints in this region (including nine long-range distance restraints and seven dihedral angle constraints) were left out. The resulting family of structures showed considerably greater disorder in loop II even when the residues making up the loop were aligned (RMSD of 1.6 Å for backbone heavy atoms). This confirms that the order observed in our original calculations is due to the experimental restraints.

Motion of loop II is consistent with the disorder observed for the loop in the crystal structure of α-cobratoxin. Rigid-body dynamics of the loop would result in apparent disorder in the crystal structure, since X-ray scattering reflects only order with respect to the unit cell, not local order.

Most of the side chain dihedral angles in loop II appear to be well ordered, although not as well ordered as the backbone dihedral angles. However, a discrepancy between observed and computed ring current shifts for the methyl group of Ala 28 provides evidence of motional averaging. A 0.48 ppm upfield ring current shift is observed, in poor agreement with the value −0.25 ppm computed (Hoch, 1983) from the structure in the ensemble that is closest to the average. Shifts calculated from other structures in the ensemble, including both ϕ 28 conformers, gave similar results. The ring current shift is caused by interaction with the rings of Trp 29, which have a similar orientation in all the structures of the ensemble. The χ_1 angle of Trp 29 is −60° and is well defined by the $H^{\alpha}-H^{\beta}$ couplings as well

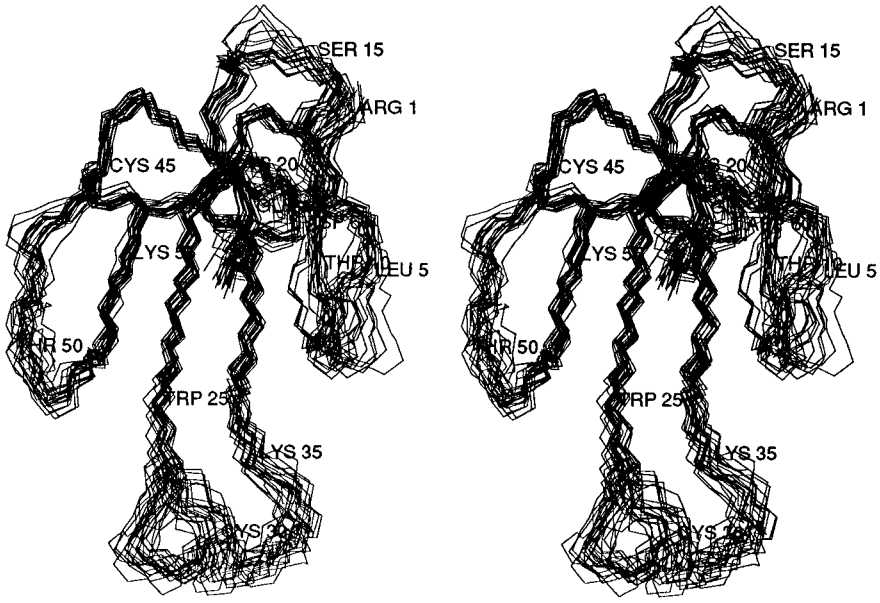

FIGURE 5: Stereoview of the least-squares superposition of N, C^{α}, and C′ (residues 1−26 and 37−62) of the 23 final refined structures of LSIII. The last four residues are disordered and are omitted for clarity.

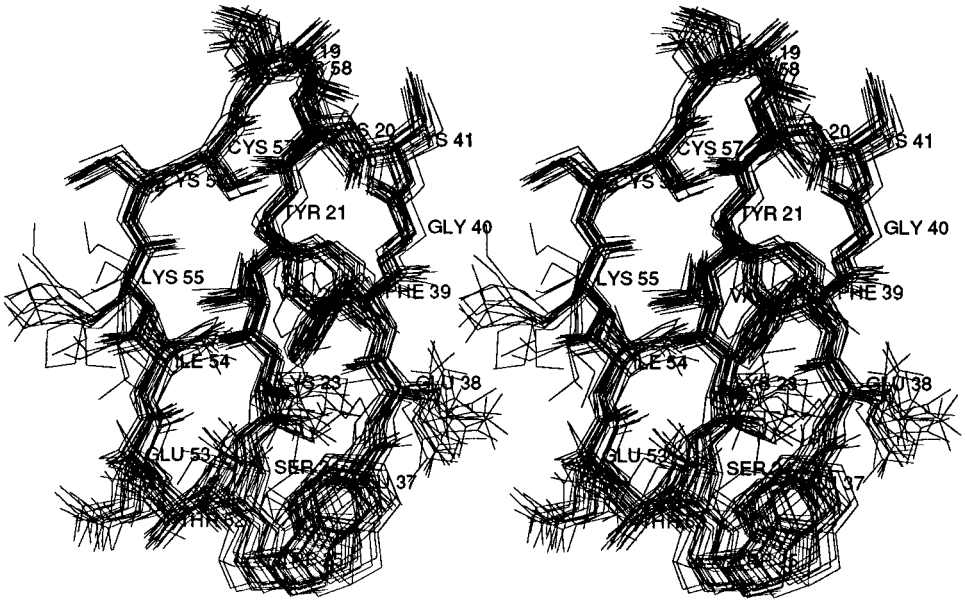

FIGURE 6: Stereoview of the least-squares superposition of all heavy atoms in the three-stranded antiparallel β-sheet (residues 19−25, 37−42, and 52−57) of LSIII.

as the $H^{N}-H^{\beta}$ and $H^{\alpha}-H^{\beta}$ NOEs. Although the χ_2 angle lies in a narrow range centered at 60°, it is not as well determined as χ_1, since it is only constrained by NOEs from 29 $H^{\alpha}-29$ H^{ϵ} and 28 $H^{\alpha}-29$ H^{δ} and not by any couplings. A grid search of the χ_2 angle showed that two of the three staggered configurations (60° and −60°) gave reasonable nonbonded energies and the third (180°) was sterically disfavored. The calculated average ring current shift of the methyl group for the two favored χ_2 angles is 0.38 ppm, in reasonable agreement with the experimental value. Although a χ_2 angle of −60° results in distance restraint violations for the two NOEs mentioned above, an r^{-6} weighted average of the two orientations results in average distances that satisfy the restraints.

Comparison to the Structures of Other Long Neurotoxins. The family of structures (Figure 5) exhibits the main structural features found in other long and short neurotoxins. The overall fold closely matches that observed in the crystal (Walkinshaw et al., 1980; Betzel et al., 1991) and solution (La Goas et al., 1992) structures of α-cobratoxin, which has 53% sequence homology with LSIII. The extent of the β-sheet strands is similar, as is the orientation of the side chains for most residues. The local structure at the end of loop II is also similar, although there is a network of hydrogen bonds in the loop of the crystal structure of α-cobratoxin that is not evident in the solution structure of LSIII. The residues in the loop exhibit large Debye−Waller factors in the crystal structure and have high RMSDs in the solution structures of both α-cobratoxin and LSIII. The side chain conformation of Phe 29 in the crystal structure of α-cobratoxin differs from that of Trp 29 in the NMR structure of LSIII. Similar chemical shifts are observed for the methyl group of Ala 28 in the NMR spectra of LSIII and α-cobratoxin, suggesting that the conformations of the aromatic sidechains at position 29 in solution are similar. The difference between the structures of loop I (residues

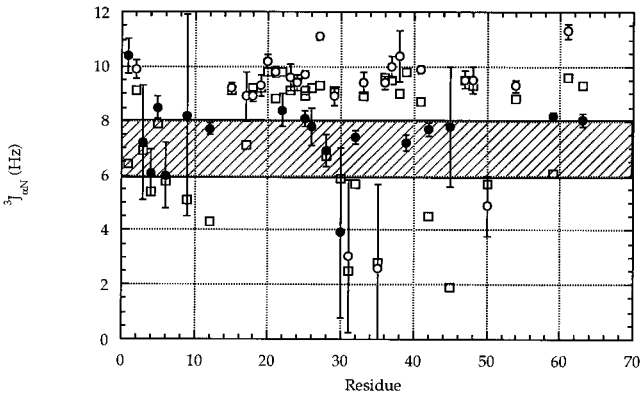

FIGURE 7: $H^{\alpha}-H^{N}$ couplings observed (○) and calculated average (□) from the final ensemble of 23 structures. Couplings lying in the range of 6−8 Hz (hatched area) were not used as restraints and are indicated by filled circles. The error bars are 1σ values calculated from the least-squares fit to the data.

Table 1: Average RMSDs between the 23 Refined Structures and the Average Structure

residues	backbone	all heavy atoms
1−60	0.94 Å	1.46 Å
1−25, 37−60	0.82 Å	1.35 Å
19−25, 37−41, 51−58 (β-sheet)	0.26 Å	0.78 Å
Restraint Violations (Average ± Standard Deviation)		
NOE		$6.14 \times 10^{-2} \pm 2.4\ 10^{-3}$ Å
dihedral		0.34 ± 0.1°
$^3J_{\alpha N}$		1.02 ± 0.1 Hz
number of distance violations > 0.3 Å		2.4 ± 0.9
$E_{L\text{-}J}$[a]		−410 ± 10 kcal/M

[a] $E_{L\text{-}J}$ is the Lennard-Jones energy of structures minimized with the CHARMM 22 potential function.

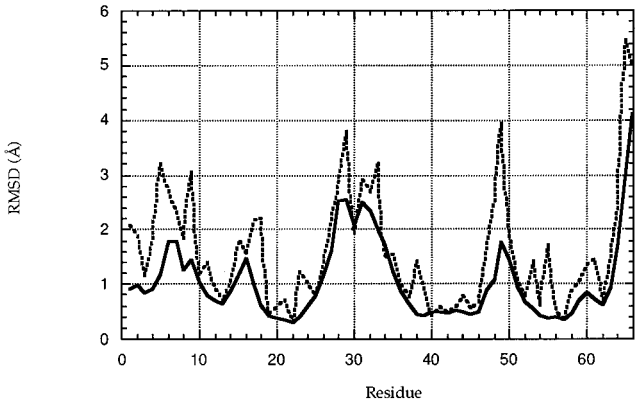

FIGURE 8: Per-residue RMS difference relative to the average structure for the final 23 refined structures of LSIII. Backbone and all heavy atom RMSDs are shown by the solid and dashed lines, respectively.

4−13) in LSIII from the corresponding loop in α-cobratoxin can be attributed to an extra residue contained in loop I of LSIII. Loop I is somewhat disordered in the solution structures of LSIII and α-cobratoxin and exhibits large Debye−Waller factors in the α-cobratoxin crystal structure.

A comparison of the crystal structure of α-bungarotoxin with the solution structure of LSIII reveals structural differences at residues 25−28 (LSIII residue numbering), where α-bungarotoxin does not form a regular β-sheet structure. The side chains of residues 25 and 27 are oriented toward the hydrophobic core of the protein in the crystal structure of α-bungarotoxin and are solvent-exposed in the solution structure of LSIII. NMR studies of α-bungarotoxin (Basus et al., 1988) indicate that the conformation of these residues in solution differs from the crystal structure and is similar to both LSIII and α-cobratoxin in solution. The side chain conformation of Phe 32 at the end of loop II is similar to that of the analogous phenylalanine in α-cobratoxin and differs from that of Trp 29 in LSIII. However, the chemical shift of the methyl group of the preceding alanine is similar to those in α-cobratoxin and LSIII, suggesting that the conformation of the aromatic residue is again similar for all three toxins in solution.

The Role of Loop II Residues in Binding to AChR. Site-directed mutagenesis and chemical modification experiments have demonstrated that many residues in loop II play an important role in the toxicity of the long neurotoxins (Endo & Tamiya, 1987). Lys 23 is believed to interact with AChR via the lysyl residue's negative charge at physiological pH. Trp 25 is conserved in all long and short neurotoxins, and its side chain is exposed to solvent. Furthermore, in several instances chemical modification of Trp 25 has resulted in reduced toxicity. It has been suggested that Trp 25 may be important in orienting the side chains at the base and tip of loop II, particularly Lys 23 and Asn 27 (Pillet et al., 1993). Our structures show that the aromatic ring of Trp 25 is packed close to the side chain of Lys 23 but does not appear to have a significant interaction with Asn 27, which is disordered with respect to the tryptophan. With only a few exceptions (of which LSIII is one), position 27 is occupied by lysine. Site-directed mutagenesis or chemical modification of this residue in short neurotoxins results in reduced toxicity, which may account for the low toxicity of LSIII relative to other neurotoxins.

The highly conserved aromatic residue at position 29 also appears to be involved in receptor binding (Pillet et al., 1993). Nonaveraged $H^{\alpha}-H^{\beta}$ couplings indicate that the χ_1 angle of Trp 29 is well defined, and it is in agreement with the χ_1 angle of Phe 29 in the X-ray structure of α-cobratoxin. As previously noted, the χ_2 angle of Trp 29 appears to adopt two different conformations. Arg 33 is also conserved in nearly all long and short neurotoxins, and it has been shown that the positive charge of the side chain is essential for efficient binding (Pillet et al., 1993). Gly 34 is found in all long and short neurotoxins, possibly for structural reasons rather than direct contact with AChR. In the crystal structure of α-cobratoxin, the backbone dihedral angles of this residue lie in a region of the Ramachandran space that would be inconsistent with any residues other than glycine. This is also true for the solution structure of LSIII.

The highly conserved disulfide bridging the binding loop presumably plays an important role in stabilizing its local structure. There are two long neurotoxins which lack this disulfide bridge: lc a and lc b from the venom of *Laticauda colubrina*. These toxins exhibit normal toxicity as measured by LD_{50}; however, LD_{50} values do not necessarily correlate well with binding constants (Martin et al., 1983). By virtue of increased exposure to solvents compared to the other disulfide bonds, it is possible to selectively reduce the disulfide bond bridging loop II (Chicheportiche et al., 1975; Martin et al., 1983). Unfortunately, the binding properties of selectively reduced toxins appear to depend on the nature of the protecting group used to prevent reoxidation of the

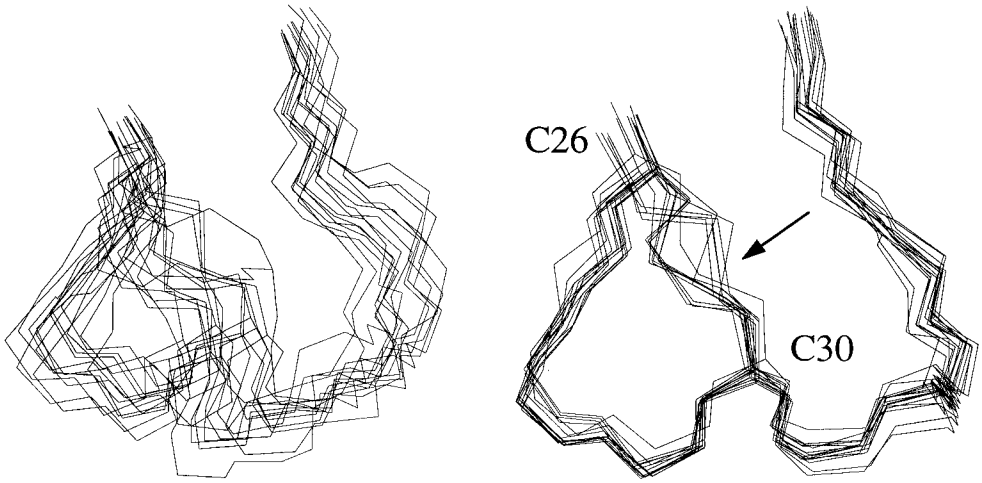

FIGURE 9: Least-squares superposition of N, C^{α}, and C′ at the end of loop II (residues 27−36) of the 23 final refined structures of LSIII (A) aligned as in Figure 4 and (B) aligned using residues 27−36 alone. The average RMSD for the residues in panel A is 1.74 Å; in panel B it is 0.44 Å. The arrow indicates the disulfide.

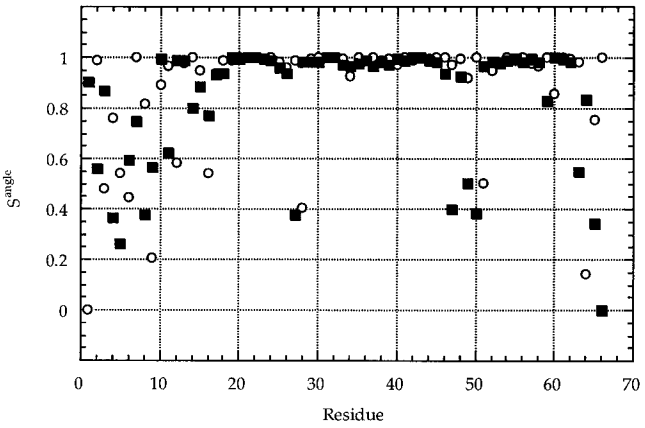

FIGURE 10: Backbone dihedral order parameters calculated from the final 23 refined structures of LSIII according to Hyberts et al. (1992). Order parameters for ϕ and ψ angles are indicated by ○ and ■, respectively.

cysteines. Thus the structural and dynamical consequences of the disulfide remain unclear.

Dynamical Implications for Binding to AChR. Previous reports of the structures of the long neurotoxins α-cobratoxin and α-bungarotoxin have shown loop II to be disordered, as revealed by high RMSDs for NMR structures and large Debye−Waller factors for X-ray structures. In contrast, our results show that the loop exhibits local order; the apparent disorder could then be a consequence of rigid-body motion of the loop with respect to the rest of the protein. This type of motion is difficult to detect in X-ray experiments, since both rigid-body motion and more general dynamical disorder of the loop would give rise to diffuse electron density. NMR studies are well suited to detecting local order, since they are based on the detection of short-range interactions. Nevertheless, the presence of local order may be obscured if structures are superimposed by least-squares matching of atoms spanning the entire protein.

The dynamics of loop II in LSIII (and related neurotoxins) may hold significance for its biological activity, since structural fluctuations can affect both kinetic and thermodynamic properties of ligand−receptor binding (Brooks et al., 1988). Mobility can lower the free energy barrier to complex formation, increasing the rate of association, by increasing the population of conformations that are favorable for binding when the average or most probable conformation is not favorable. On the other hand, too much mobility can result in an unfavorable entropy loss upon binding if the mobile regions become less mobile when bound. Searle and Williams (1992) have attempted to quantify this sort of entropy loss and have shown that it can be significant.

Conversely, a ligand that is rigid in the unbound state will lose few degrees of freedom upon binding, thus favoring complex formation. Rigid-body motion at the end of the binding loop of LSIII may represent a compromise: it allows specific groups important for binding to achieve a favorable conformation, but without so much motion that binding invokes too high an entropic cost. It is possible to speculate further about other advantages of placing residues important for binding on the end of a flexible arm, for example, as a means for reaching around an obstruction blocking access to the binding site on the surface of the receptor (Connolly et al., 1995). Further insight into the significance of the dynamics of the binding loop of LSIII can be anticipated as details of the structure of AChR and its complexes emerge (Pedersen & Cohen, 1990; Unwin, 1995).

CONCLUDING REMARKS

The solution structure of LSIII illustrates all of the structural characteristics previously observed for the family of long neurotoxins, including three loops emerging from a globular head. A characteristic not previously observed is that the prominent central loop, which contains many of the residues that are known to be important for binding to AChR, exhibits local order. Together with the pattern of vicinal coupling constants for the loop, this observation leads us to propose that the loop undergoes rigid-body motion with respect to the rest of the protein. This motion may hold significance for binding to AChR, by lowering the entropic cost of binding relative to that for a completely mobile binding loop, while still permitting some conformational flexibility to aid binding. The motion can also explain the apparent disorder observed for the central loop in prior X-ray and NMR studies of long neurotoxins and may be a general characteristic of all long neurotoxins. Further insights into the nature of the motion and its role in binding to AChR could be obtained from relaxation studies and from studies of neurotoxins lacking the loop-bridging disulfide. Rigid-

body motion of binding loops has been observed in other proteins, such as eglin *c* (Peng & Wagner, 1992), and may be a more general feature of protein recognition than has been recognized. The prevalence of such motions should become clearer as more NMR studies emerge, since X-ray studies are not well suited to detecting the presence of this type of motion, in contrast to NMR experiments, which specifically detect local, short-range order.

ACKNOWLEDGMENT

We thank Molecular Simulations Inc. for the use of their software and Axel Brünger for providing us with the *J* restraint code for X-PLOR. We also thank Jonathan Moore, Michael Nilges, Abraham Szöke, and Gerhard Wagner for helpful discussions.

SUPPORTING INFORMATION AVAILABLE

A table giving the proton assignments for LSIII at pH 4.6 and 25 °C (3 pages). Ordering information is given on any current masthead page.

REFERENCES

Basus, V. J., Billeter, M., Love, R. A., Stroud, R. M., & Kuntz, I. D. (1988) *Biochemistry 27,* 2763−2771.
Bax, A., & Drobny, G. (1985) *J. Magn. Reson. 61,* 306−320.
Betzel, C., Lange, G., Pal, G. P., Wilson, K. S., Maelicke, A., & Saenger, W. (1991) *J. Biol. Chem. 266,* 21530−21536.
Brooks, C. L., Karplus, M., & Pettit, B. M. (1988) *Proteins: A Theoretical Perspective of Dynamics, Structure, and Thermodynamics,* Wiley, New York.
Brünger, A. T. (1992) *X-PLOR Version 3.1 Manual,* Yale University, New Haven CT.
Cavanagh, J., & Rance, M. (1990) *J. Magn. Reson. 88,* 72−85.
Chicheportiche, R., Vincent, J.-P., Kopeyan, C., Schweitz, H., & Lazdunski, M. (1975) *Biochemistry 14,* 2081−2091.
Connolly, P. J., Stern, A. S., & Hoch, J. C. (1994) *J. Am. Chem. Soc. 116,* 2675−2676.
Connolly, P. J., Stern, A. S., & Hoch, J. C. (1995) in *Dynamics and the Problem of Recognition in Biological Macromolecules* (Jardetzky, O., & Lefèvre, J.-F., Eds.) Plenum Press, New York.
Eccles, C., Güntert, P., Billeter, M., & Wüthrich, K. (1991) *J. Biol. NMR 1,* 111−130.
Eich, G., Bodenhausen, G., & Ernst, R. R. (1982) *J. Am. Chem. Soc. 104,* 3731−3732.
Endo, T., & Tamiya, N. (1987) *Pharmacol. Ther. 34,* 403−451.
Griesinger, C., Sørensen, O. W., & Ernst, R. R. (1985) *J. Am. Chem. Soc. 107,* 6394−6396.
Güntert, P., Braun, W., & Wüthrich, K. (1991) *J. Mol. Biol. 317,* 517−530.
Hoch, J. C. (1983) Ph.D. Thesis, Harvard University.
Hoch, J. C., & Stern, A. S. (1992) *J. Biomol. NMR 2,* 535−543.
Hoch, J. C., & Stern, A. S. (1993) *The Rowland NMR Toolkit V3,* Rowland Institute for Science, Cambridge, MA.
Hoch, J. C., Dobson, C. M., & Karplus, M. (1985) *Biochemistry 24,* 3831−3841.
Hyberts, S. G., Goldberg, M. S., Havel, T. F., & Wagner, G. (1992) *Protein Sci. 1,*
736−751.
Kumar, A., Ernst, R. R., & Wüthrich, K. (1980) *Biochem. Biophys. Res. Commun. 95,* 1−6.
LaGoas, R., LaPlante, S. R., Mikou, A., Delsuc, M.-A., Guittet, E., Robin, M., Charpenteir, I., & Lallemand, J.-Y. (1992) *Biochemistry 31,* 4867−4875.
Love, R. A., & Stroud, R. M. (1986) *Protein Eng. 1,* 37−46.
Marion, D., & Wüthrich, K. (1983) *Biochem. Biophys. Res. Commun. 113,* 967−974.
Marion, D., & Bax, A. (1988) *J. Magn. Reson. 80,* 528−533.
Marion, D., Ikura, M., & Bax, A. (1989) *J. Magn. Reson. 84,* 425−430.
Martin, B. M., Chibber, B. A., & Maelicke, A. (1983) *J. Biol. Chem. 252,* 8714−8722.
Molecular Simulations Inc. (1994) *Quanta 4.0 Manual,* Burlington, MA.
Nilges, M., Gronenborn, A. M., & Clore, G. M. (1988) *FEBS Lett. 229,* 313−324.
Piantini, U., Sørensen, O. W., & Ernst, R. R. (1982) *J. Am. Chem. Soc. 104,* 6800−6801.
Pedersen, S. P., & Cohen, J. B. (1990) *Proc. Natl. Acad. Sci. U.S.A. 87,* 2785−2789.
Peng, J. W., & Wagner, G. (1992) *Biochemistry 31,* 8571−8586.
Pillet, L., Trémeau, O., Ducancel, F., Drevet, P., Zinn-Justin, S., Pinkasfeld, S., Boulain, J.-C., & Ménez, A. (1993) *J. Biol. Chem. 268,* 909−916.
Plateau, P., & Guèron, M. (1982) *J. Am. Chem. Soc. 104,* 7310−7311.
Rance, M. (1987) *J. Magn. Reson. 74,* 557−564.
Rance, M., Sørensen, O. W., Bodenhausen, G., Wagner, G., Ernst, R. R., & Wüthrich, K. (1983) *Biochem. Biophys. Res. Commun. 117,* 479−485.
Rucker, S. P., & Shaka, A. J., (1989) *Mol. Phys. 68,* 509−517.
Searle, M. S., & Williams, D. H. (1992) *J. Am. Chem. Soc. 114,* 10690−10697.
Shaka, A. J., & Freeman, R. (1983) *J. Magn. Reson. 51,* 169−173.
States, D. J., Haberkorn, R. A., & Ruben, D. J. (1982) *J. Magn. Reson. 48,* 286−292.
Stern, A. S. (1994) *XPEAKFIT,* The Rowland Institute for Science, Cambridge, MA.
Unwin, N. (1995) *Nature 373,* 37−43.
Vuister, G. W., Boelens, R., & Kaptein, R. (1988) *J. Magn. Reson. 80,* 176−185.
Wagner, G. (1983) *J. Magn. Reson. 55,* 151−156.
Walkinshaw, M. D., Saenger, W., & Maelicke, A. (1980) *Proc. Natl. Acad. Sci. U.S.A. 72,* 2400−2404.
Wüthrich, K. (1986) *NMR of Proteins and Nucleic Acids,* Wiley, New York.
Wüthrich, K., Billeter, M., & Braun, W. (1983) *J. Mol. Biol. 169,* 949−961.

BI9520287